

Gate-Controlled Spin-Orbit Quantum Interference Effects in Lateral Transport

J. B. Miller,^{1,2} D. M. Zumbühl,¹ C. M. Marcus,¹ Y. B. Lyanda-Geller,³
D. Goldhaber-Gordon,^{1,4} K. Campman,⁵ and A. C. Gossard⁵

¹Department of Physics, Harvard University, Cambridge, Massachusetts 02138

²Division of Engineering and Applied Science, Harvard University, Cambridge, Massachusetts 02138

³Naval Research Laboratory, Washington, D.C. 20375

⁴Department of Physics, Stanford University, Stanford, California 94305

⁵Materials Department, University of California at Santa Barbara, Santa Barbara, California, 93106

In situ control of spin-orbit coupling in coherent transport using a clean GaAs/AlGaAs two-dimensional electron gas is realized, leading to a gate-tunable crossover from weak localization to antilocalization. The necessary theory of 2D magnetotransport in the presence of spin-orbit coupling beyond the diffusive approximation is developed and used to analyze experimental data. With this theory the Rashba contribution and linear and cubic Dresselhaus contributions to spin-orbit coupling are separately estimated, allowing the angular dependence of spin-orbit precession to be extracted at various gate voltages.

An important component along the path toward realizing quantum “spintronic” devices [1, 2] is a structure that allows manipulation of electron spin without destroying phase coherence. Spin-orbit (SO) coupling has been the focus of recent studies because of its potentially useful role in coherent spin rotators [3], spin interference devices [4], and spin-filters [5, 6]. The mechanisms by which SO coupling affects transport [7, 8, 9, 10] have recently been considered in the context of Aharonov-Bohm (AB) phase and Berry phase [4, 11, 12, 13, 14, 15, 16], underscoring the richness of the underlying physics.

The conductivity of low-dimensional systems shows signatures of quantum interference that depend on magnetic field and SO coupling [7, 8, 17, 18, 19]. In particular, constructive (destructive) backscattering associated with pairs of time-reversed closed-loop electron trajectories in the absence (presence) of significant SO interaction leads to negative (positive) magnetoresistance effects known as weak localization (antilocalization) [9]. In this Letter, we demonstrate *in situ* control of SO coupling in a moderately high mobility GaAs/AlGaAs two-dimensional electron gas (2DEG), inducing a crossover from weak localization (WL) to antilocalization (AL) as a function of an applied top-gate voltage (see Fig. 1). Theory beyond the diffusive approximation must be used to extract gate-voltage-dependent SO parameters from magnetotransport when the SO precession frequency becomes comparable to the inverse transport scattering time (τ^{-1}) as occurs here, and when the magnetic length becomes comparable to the mean free path. Theory that accounts for AB-like spin phases and spin-relaxation [20] is developed here and used to estimate *separately* the various SO terms (Rashba, linear and cubic Dresselhaus) over a range of gate voltages, ranging from WL to AL. Conventional WL theories assume SO times much longer than τ [7, 8, 13] and so cannot be applied to clean materials. Previous theories that go beyond the diffusive approximation do not treat SO [21, 22], or treat it only as spin-relaxation [23, 24] without accounting for Berry

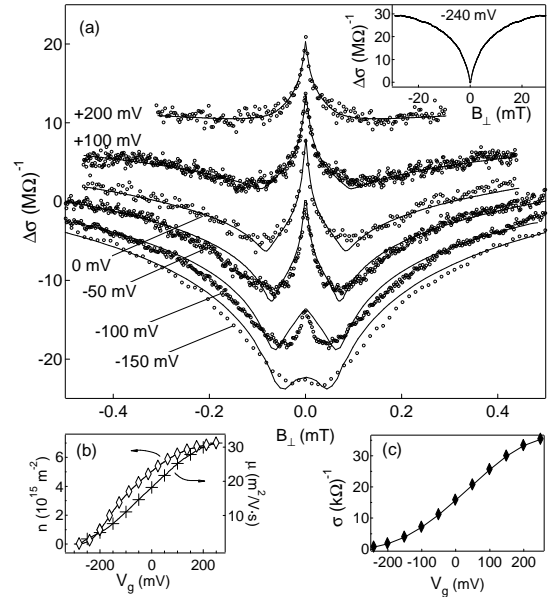


FIG. 1: (a) Experimental magnetoconductance, $\Delta\sigma = \sigma(B) - \sigma(0)$, (circles) offset for clarity, along with three-parameter fits to Eq. (2) (solid curves) for several gate voltages. Inset: Experimental magnetoconductance data for the most negative gate voltage, showing pure WL. (b) Density and mobility as a function of V_g , extracted from longitudinal and Hall voltage measurements. (c) Experimental conductivity, showing strong dependence on V_g . Note that $\Delta\sigma \sim 10^{-3}\sigma$.

phase effects which play a crucial role, as we show here. Previous experiments in which SO rates are measured using WL/AL in a gated GaAs heterostructure have not reported *in situ* gate control [10, 25, 26]. Koga *et al.* [27] demonstrated gate controlled SO coupling in InGaAs heterostructures using WL/AL. Modification of Rashba SO coupling using gated quantum wells has been observed using beating patterns in Shubnikov-de Haas oscillations in InGaAs [28, 29], InAs/AlSb [30] and HgTe [31]. Gate controlled SO coupling in GaAs 2D hole systems [32, 33, 34] has also been investigated using beating

of Shubnikov-de Haas oscillations. The angular variation of SO coupling in GaAs quantum wells has been measured using Raman scattering [35].

The Hamiltonian for conduction band electrons in a [001] 2DEG is $\mathcal{H} = \frac{\hbar^2 k^2}{2m^*} + (\boldsymbol{\sigma} \cdot \boldsymbol{\Omega})$, where m^* is the effective mass, $k = |\mathbf{k}|$ ($\mathbf{k} = (k_x, k_y)$) is the in-plane wave vector, $\boldsymbol{\sigma} = (\sigma_x, \sigma_y, \sigma_z)$ is the Pauli spin operator and $\boldsymbol{\Omega} = (\Omega_x, \Omega_y)$ is the total SO frequency. $\boldsymbol{\Omega}$ can be written as the vector sum of linear ($\boldsymbol{\Omega}_{D1}$) and cubic ($\boldsymbol{\Omega}_{D3}$) Dresselhaus terms and the Rashba term ($\boldsymbol{\Omega}_R$),

$$\boldsymbol{\Omega}_{D1} = \alpha_1 (-\hat{\mathbf{x}}k_x + \hat{\mathbf{y}}k_y)/\hbar, \quad (1a)$$

$$\boldsymbol{\Omega}_R = \alpha_2 (\hat{\mathbf{x}}k_y - \hat{\mathbf{y}}k_x)/\hbar, \quad (1b)$$

$$\boldsymbol{\Omega}_{D3} = \gamma (\hat{\mathbf{x}}k_x k_y^2 - \hat{\mathbf{y}}k_x^2 k_y)/\hbar. \quad (1c)$$

where γ arises from the lack of inversion symmetry of the GaAs crystal, while $\alpha_1 = \gamma \langle k_z^2 \rangle$ also depends on the thickness of the wave function in the quantization direction. α_2 depends on the potential profile of the heterointerface. We assume the effect of gate voltage, V_g , on Ω ($\equiv |\boldsymbol{\Omega}|$) is through the carrier density, $n = k^2/2\pi$. Previous studies of SO coupling in single-interface heterostructures [36] support this assumption. The magnitude of α_2 in a single-interface heterostructure originates mainly from the band-offset at the heterointerface, which is roughly independent of V_g [30, 37]. The symmetry of the linear (in k) SO terms, $\boldsymbol{\Omega}_{D1}$ and $\boldsymbol{\Omega}_R$, allows these terms to be represented as a spin-dependent vector potential \mathbf{A} that affects the orbital motion and phase of electrons, $\boldsymbol{\sigma} \cdot (\boldsymbol{\Omega}_{D1} + \boldsymbol{\Omega}_R) \propto \mathbf{k} \cdot \mathbf{A}$ [4, 11, 12, 13, 14, 15]. That is, the linear terms affect electronic interference as a spin-dependent AB-like effect. In contrast, the cubic term, Eq. (1c), upon removing terms with the symmetry of Eq. (1a), only causes spin relaxation in the diffusive regime (although it also can produce AB-like effects in the quasi-ballistic regime [4]). To develop the theory of 2D magnetotransport with SO coupling beyond the diffusive approximation [20], we follow Refs. [21, 22, 23], which treat the quasi-ballistic case $\ell_B < \ell$ ($\ell_B = \sqrt{\hbar/2eB}$ is the magnetic length and ℓ is the transport mean free path) without SO coupling. The approach is to introduce an operator $P = G_{\epsilon+\omega}^R(\mathbf{r}_1, \mathbf{r}_2, \sigma_1) G_{\epsilon}^A(\mathbf{r}_1, \mathbf{r}_2, \sigma_2) \hbar/2\pi\nu\tau$ for the probability of an electron to propagate both forward and backward along a path segment from \mathbf{r}_1 to \mathbf{r}_2 , where G^R (G^A) are single-electron retarded (advanced) Green functions, $\sigma_{1(2)}$ are the Pauli spin operators for particle moving forward (backward), ν is the density of states per spin, and τ is the scattering time. The interference contribution from traversing a closed trajectory with n scattering events is given by the trace of $(P)^n$. In the presence of SO coupling, Eq. (1), the formulas in [22] remain valid once a summation over spins is included in the trace. Introducing the total spin of interfering particle waves, $\mathbf{S} = \sigma_1 + \sigma_2$, we write $\text{Tr}[(P)^n] = \frac{1}{2}\text{Tr}[(P_1)^n - (P_0)^n]$, where operators P_0 and P_1 describe singlet ($S = 0$) and

triplet ($S = 1$) contributions. To calculate $\text{Tr}[(P_{0(1)})^n]$, we diagonalize $P_{0(1)}$. We find that when $\boldsymbol{\Omega}_{D1}$ and $\boldsymbol{\Omega}_R$ are taken into account, $P_{0(1)}$ has the same eigenfunctions as the Hamiltonian \mathcal{H} for particles with charge $2e$, spin \mathbf{S} and spin frequency $2\boldsymbol{\Omega}$: $\mathcal{H} = \frac{\hbar^2}{2m^*}(\mathbf{k} - 2e\mathbf{A}_{em} + 2e\mathbf{A}_S)^2$, where \mathbf{A}_{em} is the vector potential associated with the applied perpendicular magnetic field, B , and $\mathbf{A}_S = \frac{m^*}{2e\hbar^3}(-\alpha_1 S_x - \alpha_2 S_y, \alpha_2 S_x + \alpha_1 S_y)$ is the SO vector potential. For $S = 0$, the eigenstates are Landau levels for a charge $2e$ particle in the magnetic field B , analogous to the spinless problem [23]. For $S = 1$, eigenstates of \mathcal{H} and P_1 in general require a numerical solution, although analytic solutions exist when either α_1 or α_2 equals zero [20]. An analytic solution is also found for $\alpha_1, \alpha_2 \neq 0$, when $\ell_B < \lambda_{so}$, where $\lambda_{so} = (2\alpha_{1(2)}m^*/\hbar^2)^{-1}$ is the distance over which spin rotates appreciably (if $\ell > \lambda_{so}$) or dephases (if $\ell < \lambda_{so}$) due to spin AB-like effects. Performing a unitary transformation $\mathcal{H} \rightarrow \tilde{\mathcal{H}} = U^\dagger \mathcal{H} U$, with $U = \exp(-ie\mathbf{A}_S \cdot \mathbf{r})$, and expanding in coordinates, we find $\tilde{\mathcal{H}} = \frac{\hbar^2}{2m^*}(\mathbf{k} - 2e\mathbf{A}_{em} + S_z \mathbf{a})^2$, where $\mathbf{a} = H_{\text{eff}} \mathbf{r} \times \hat{\mathbf{z}}/(2\hbar^2)$, and $H_{\text{eff}} = 2(\alpha_2^2 - \alpha_1^2)m^{*2}/e\hbar^3$ is the effective SO field. P_1 can then be block-diagonalized for each m ($m = 0, \pm 1$) using the Landau basis for particles with charge $2e$ in the magnetic field $B - mH_{\text{eff}}$. Thus, the effect of $\boldsymbol{\Omega}_{D1}$ and $\boldsymbol{\Omega}_R$ is to produce AB-like spin phases [4, 11, 12, 13, 14, 15]. Higher expansion terms to $\tilde{\mathcal{H}}$ describe spin flip processes and can be taken into account by introducing a spin relaxation time τ_{so} and its corresponding field scale $H_{so} = \hbar\tau/(2e\ell^2\tau_{so})$. The resulting quantum interference contribution takes the form [20]

$$\Delta\sigma(B) = -\frac{e^2}{4\pi^2\hbar} \left[\sum_{m=-1,0,1} C(x_{1m}, f_{1m}) - C(x_{00}, f_{00}) \right] \quad (2)$$

where $x_{Sm} = (B - mH_{\text{eff}})/H_{tr}$ describes the AB dephasing in H_{eff} , $C(x, f_{Sm}) = x \sum_{N=0}^{\infty} \frac{P_N^3(f_{Sm})}{1 - P_N(f_{Sm})}$, $P_N(f_{Sm}) = y \int_0^{\infty} \exp(-y f_{Sm} t - t^2/2) L_N(t^2) dt$, $L_N(z)$ are Laguerre polynomials, $y = (2/|x|)^{1/2}$, and $H_{tr} = \hbar/(2e\ell^2)$. The dephasing factors f_{Sm} are given by $f_{1\pm 1} = (1 + (H_\varphi + H_{so})/H_{tr})$; $f_{00} = (1 + H_\varphi/H_{tr})$; $f_{10} = (1 + (H_\varphi + 2H_{so})/H_{tr})$, where $H_\varphi = \hbar/(4eL_\varphi^2)$ and L_φ is the phase breaking length. Equation (2) does not include all B -dependent interference terms, notably excluding Cooper-channel contributions due to electron-electron interactions [18] and a reduction of WL due to electron diffraction effects [21]. Also, in an attempt to capture the effects of cubic terms on H_{eff} and H_{so} , we introduce an effective vector potential $\mathbf{A}_S^* = \mathbf{A}_S + \gamma \frac{m^*}{e\hbar^2}(k_y^2, -k_x^2) \sim \mathbf{A}_S + \gamma \frac{m^*}{2e\hbar^2}(k^2, -k^2)$ which leads to an effective SO field,

$$H_{\text{eff}}^* = 2(\alpha_2^2 - \alpha_1^2 + 2\pi n \alpha_1 \gamma - \pi^2 \gamma^2 n^2) m^{*2}/e\hbar^3. \quad (3)$$

Equation (2) is applicable when $B > H_{\text{eff}}^*$ (see Fig 2). We have confirmed that fitting only to data where $B > H_{\text{eff}}^*$

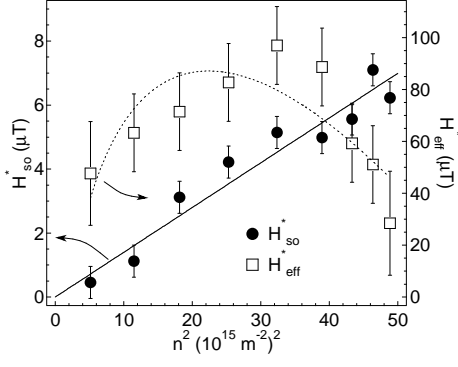


FIG. 2: Spin-orbit effective fields, H_{so}^* (filled circles) and H_{eff}^* (open squares), as extracted using Eq. (2), plotted as a function of sheet density squared. The best fit of Eq. (3) to H_{eff}^* (dotted curve) is used to extract γ , α_1 and α_2 . Alternatively, the best linear fit to H_{so}^* (solid line) is used to extract γ .

gives, within error bars, the same results as fitting over the entire measured range of B . Modification of the commutator $[\mathbf{k} + 2e\mathbf{A}_S^*, \mathbf{r}]$ by \mathbf{A}_S^* induces spin flipping terms $\sim \gamma k^3/4$ in the transformed Hamiltonian $\tilde{\mathcal{H}}^*$. The corresponding $H_{so}^* = \frac{1}{36}\pi^2 m^{*2} \gamma^2 n^2 / e\hbar$, using its expression in the diffusive regime.

We now turn to a discussion of the experiment. Samples on three separate heterostructure materials all showed qualitatively similar behavior. The sample for which data is presented consists of a GaAs/AlGaAs heterostructure grown in the [001] direction with double δ -doping layers set back 143 Å and 161 Å from the 2DEG and a total distance of 349 Å from the surface to the 2DEG. A 200 μm wide Hall bar with 700 μm between voltage probes was patterned by wet etching. A lithographically defined Cr/Au top gate was used to control density and mobility in the Hall bar over the range $n = 1.4\text{--}7.0 \times 10^{15} \text{ m}^{-2}$ and $\mu = 3.6\text{--}31 \text{ m}^2/\text{Vs}$. Measurements were made in a ^3He cryostat at temperature $T = 300 \text{ mK}$ using ac lock-in techniques with bias currents ranging from 50 to 500 nA. Figure 1(a) shows the longitudinal magnetoconductance as a function of V_g . A crossover from pure WL (Fig. 1(a), inset) at $V_g = -240 \text{ mV}$ to essentially pure AL at $V_g = +250 \text{ mV}$ is observed. This crossover demonstrates that a gate can be used to control SO over a wide range, as pure WL corresponds to negligible SO rotations within the phase coherence length L_ϕ , while AL corresponds to spin rotations $\gtrsim 2\pi$. The solid curves in Fig. 1(a) are fits to Eq. (2) with three free parameters, H_ϕ , H_{so}^* , and H_{eff}^* . H_{tr} is fixed at each gate voltage by measured values of density and mobility. Figure 2 shows extracted parameters H_{so}^* and H_{eff}^* as a function of n^2 . H_{so}^* is well described by the predicted linear dependence on n^2 , with a best fit (Fig. 2, solid line) giving $\gamma = 31 \pm 3 \text{ eV}\text{\AA}^3$ with zero y-intercept (see Eq. (1c)). The density dependence of H_{eff}^* is well described by Eq. (3), (Fig. 2, dotted curve), giving fit parameters $\gamma = 28 \pm 4 \text{ eV}\text{\AA}^3$, $\alpha_1 = 4 \pm 1 \text{ meV}\text{\AA}$ and $\alpha_2 = 5 \pm 1 \text{ meV}\text{\AA}$. In this way, the three SO parameters α_1 , α_2 , and γ are separately obtained from transport measurements by explicitly making use of the density de-

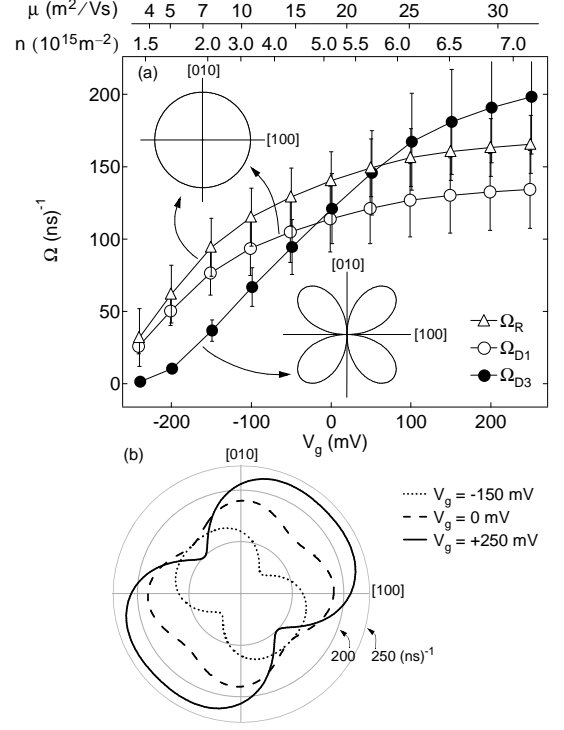


FIG. 3: (a) Magnitudes of isotropic linear Dresselhaus (Ω_{D1}) and Rashba (Ω_R) terms, and nonisotropic cubic Dresselhaus (Ω_{D3}) term as functions of gate voltage, V_g , density, n , and mobility, μ . Insets show theoretical dependence on momentum direction for the three terms, indicating that the linear terms are isotropic, while the cubic term has a four-fold symmetry and is highly anisotropic. Maximum magnitude (when $\phi = (j + \frac{1}{4})\pi$) is shown for the anisotropic (Ω_{D3}) term. (b) Angular variation of Ω , the magnitude of the total SO precession vector at $V_g = -150 \text{ mV}$ (dotted), 0 mV (dashed), and 250 mV (solid), corresponding to densities of 2.3 , 5.0 , and $7.0 \times 10^{15} \text{ m}^{-2}$ respectively.

pendence of H_{eff}^* and H_{so}^* . Extracted values of H_ϕ correspond to dephasing times in the range $\tau_\phi \sim 0.1\text{--}1.0 \text{ ns}$ at 300 mK , which decrease by more than an order of magnitude as temperature is increased to 2.5 K . Within the error bars, H_{so}^* and H_{eff}^* do not depend on temperature over this temperature range. Figure 3(a) displays the magnitudes of the three spin-orbit terms as functions of V_g , n , and μ , determined using Eq. (1) and the extracted values of α_1 , α_2 , and γ . Plotted are values along the [110] direction, $\phi \equiv \tan^{-1}(k_y/k_x) = \frac{\pi}{4}$, where Ω_{D3} is maximum. The total spin precession rate, Ω , is plotted as a function of the direction, ϕ , of the electron momentum in Fig. 3(b). While for most directions Ω is an increasing function of density, it is seen to decrease with increasing density near $\phi = \frac{3\pi}{4}$ and $\frac{7\pi}{4}$. The linear Dresselhaus and Rashba terms (Ω_{D1} and Ω_R) are of comparable magnitude to each other for all densities and in all directions. Near $\phi = \frac{j\pi}{2}$ (j an integer), $\Omega_{D3} \ll \Omega_{D1}, \Omega_R$ and the SO is controlled by the linear terms. For ϕ near $\frac{(2j+1)\pi}{4}$, the cubic term becomes comparable to or even exceeds (at high densities) the linear terms. Depending on ϕ , the linear and cubic terms either add ($\phi \sim \frac{\pi}{4}, \frac{5\pi}{4}$) or subtract ($\phi \sim \frac{3\pi}{4}, \frac{7\pi}{4}$). The extracted values for γ ($31 \pm 3 \text{ eV}\text{\AA}^3$) us-

ing H_{so}^* , $28 \pm 4 \text{ eV}\text{\AA}^3$ using H_{eff}^*) are in good agreement with the value $27.5 \text{ eV}\text{\AA}^3$ from band structure calculations [36, 37]. Values of Ω are $\sim 3 - 8$ times smaller than previously measured using Shubnikov-deHaas oscillations [26], with corresponding theory [26, 37] lying roughly between the experimental ranges. We note, however, that the values are sample dependent. Estimates for α_1 give values for $\langle k_z^2 \rangle$ that correspond to a wave function width of $\sim 10 \text{ nm}$ in the \hat{z} direction, which is also reasonable. The extracted α_2 corresponds to a uniform electric field $E \sim 10 \text{ MV/m}$, using $\alpha_2 = \alpha_0 e E$ and a value of $\alpha_0 = 5.33 \text{ \AA}^2$ from a $\mathbf{k} \cdot \mathbf{p}$ model [36, 37]. Previously existing models for WL/AL [8, 13, 36] provide fits to the data that appear qualitatively reasonable, giving values for H_{so} that are ~ 5 times higher than those found using Eq. (2). However, these fits also lead to the unphysical result that $\tau_{so} < \tau$. Such unphysical results are not surprising given that, for $V_g > -50 \text{ mV}$, the SO length, $v_F/\langle \Omega \rangle$, is less than ℓ , while theory [8, 13, 36] assumes diffusive spin evolution $\ell \ll \lambda_{so}, L_\varphi$. We note that a theory for arbitrarily strong SO coupling [14] may also be used to fit this data by including B via L_φ . This approach yields values for Ω_{D3} and Ω_{D1} consistent with Eq. (2) to within a factor of ~ 3 , but does not separate Ω_{D1} and Ω_R terms. We thank I. Aleiner, H. Bruus and S. Studenikin for illuminating discussions and F. Mancoff for device fabrication. This work was supported in part by DARPA-QuIST, DARPA-SpinS, ARO-MURI, and NSF-NSEC. We also acknowledge support from ONR and NSA (Y. L.-G.), NDSEG (J. B. M.) and the Harvard Society of Fellows (D.G.-G). Work at UCSB was supported by QUEST, an NSF Science and Technology Center.

-
- [1] S. A. Wolf et al., *Science* **294**, 1488 (2001).
 - [2] D. D. Awschalom et al., *Semiconductor Spintronics and Quantum Computation* (Springer-Verlag, 2002).
 - [3] S. Datta and B. Das, *Appl. Phys. Lett.* **56**, 665 (1990).
 - [4] A. G. Aronov and Y. B. Lyanda-Geller, *Phys. Rev. Lett.* **70**, 343 (1993).

- [5] T. Koga et al., *Phys. Rev. Lett.* **88**, 126601 (2002).
- [6] A. Kiselev and K. Kim, *Appl. Phys. Lett.* **78**, 775 (2001).
- [7] S. Hikami et al., *Prog. Theor. Phys.* **63**, 707 (1980).
- [8] B. Altshuler et al., *JETP* **54**, 411 (1981).
- [9] G. Bergmann, *Phys. Rep.* **107**, 1 (1984).
- [10] P. D. Dresselhaus et al., *Phys. Rev. Lett.* **68**, 106 (1992).
- [11] H. Mathur and A. D. Stone, *Phys. Rev. Lett.* **68**, 2964 (1992).
- [12] Y. B. Lyanda-Geller and A. D. Mirlin, *Phys. Rev. Lett.* **72**, 1894 (1994).
- [13] S. V. Iordanskii et al., *JETP Lett.* **60**, 206 (1994).
- [14] Y. Lyanda-Geller, *Phys. Rev. Lett.* **80**, 4273 (1998).
- [15] I. L. Aleiner and V. I. Fal'ko, *Phys. Rev. Lett.* **87**, 256801 (2001).
- [16] D. M. Zumbühl et al., *Phys. Rev. Lett.* **89**, 276803 (2002).
- [17] E. Abrahams et al., *Phys. Rev. Lett.* **42**, 673 (1979).
- [18] B. L. Altshuler and A. G. Aronov, *Electron-Electron Interactions in Disordered Systems*, ed by A. L. Efros and M. Pollak (North Holland, Amsterdam, 1985), p. 11.
- [19] L. Gorkov et al., *JETP Lett.* **30**, 228 (1980).
- [20] Y. Lyanda-Geller (2002), unpublished.
- [21] V. M. Gasparyan and A. Y. Zyuzin, *Sov. Phys. Solid State* **27**, 999 (1985).
- [22] A. Cassam-Chenai and B. Shapiro, *J. Phys. I* **4**, 1527 (1994).
- [23] A. Kawabata, *J. Phys. Soc. Jpn.* **53**, 3540 (1984).
- [24] A. Zduniak et al., *Phys. Rev. B* **56**, 1996 (1997).
- [25] J. E. Hansen et al., *Phys. Rev. B* **47**, 16040 (1993).
- [26] P. Ramvall et al., *Phys. Rev. B* **55**, 7160 (1997).
- [27] T. Koga et al., *Phys. Rev. Lett.* **89**, 046801 (2002).
- [28] J. Nitta et al., *Phys. Rev. Lett.* **78**, 1335 (1997).
- [29] T. Schäpers et al., *J. Appl. Phys.* **83**, 4324 (1998).
- [30] J. P. Heida et al., *Phys. Rev. B* **57**, 11911 (1998).
- [31] M. Schultz et al., *Semicond. Sci. Technol.* **11**, 1168 (1996).
- [32] S. J. Papadakis et al., *Physica E* **9**, 31 (2001).
- [33] R. Winkler et al., *Phys. Rev. B* **65**, 155303 (2002).
- [34] J. P. Lu et al., *Phys. Rev. Lett.* **81**, 1282 (1998).
- [35] B. Jusserand et al., *Phys. Rev. B* **51**, 4707 (1995).
- [36] W. Knap et al., *Phys. Rev. B* **53**, 628 (1996).
- [37] P. Pfeffer, *Phys. Rev. B* **59**, 15902 (1999).